Supplemental Table 1

Mouse model			
Kidneys (n=10)	CLI	FAR-CLI	p-value
Activity in kBq/ml Median (IQR)	339.58 (303.67; 391.12)	296.38 (268.97, 361.94)	n.s.
CNR Median (IQR)	15.85 (9.15; 22.06)	16.12 (8.71, 22.78)	n.s.
Prostate cancer (n=5)	CLI	FAR-CLI	
Activity in kBq/ml Median (IQR)	29.23 (26.26, 36.21)	26.92 (22.85, 33.45)	n.s.
CNR Median (IQR)	3.33 (2.05, 4.18)	4.1 (3.03, 12.03)	n.s.
Kidneys / Prostate cancer			
Kidneys (n=10)	CLI	FAR-CLI	p-value
Activity in kBq/ml Median (IQR)	113.85 (98.65, 134.93)	103.56 (85.82, 121.3)	n.s.
CNR Median (IQR)	21.29 (17.8, 29.12)	28.68 (26.32, 47.25)	0.04
Prostate cancer (n=5)	CLI	FAR-CLI	
Activity in kBq/ml Median (IQR)	9.92 (8.61, 12.71)	9.03 (7.63, 11.36)	n.s.
CNR Median (IQR)	1.16 (0.77, 1.89)	13.7 (8.97, 20.65)	0.009

Cerenkov luminescence and flexible autoradiography imaging measurements of the mouse model and the kidneys / prostate cancer tissue with the corresponding activity levels. Measured intensities are stated as contrast to noise ratio (CNR). All data are given as median and interquartile range. Significance was set at $p<0.05$. FAR: Flexible Autoradiography, CLI: Cerenkov Luminescence Imaging, CNR: Contrast-to-noise-ratio, IQR: Interquartile range, n.s.: not significant

Supplemental Figure 1

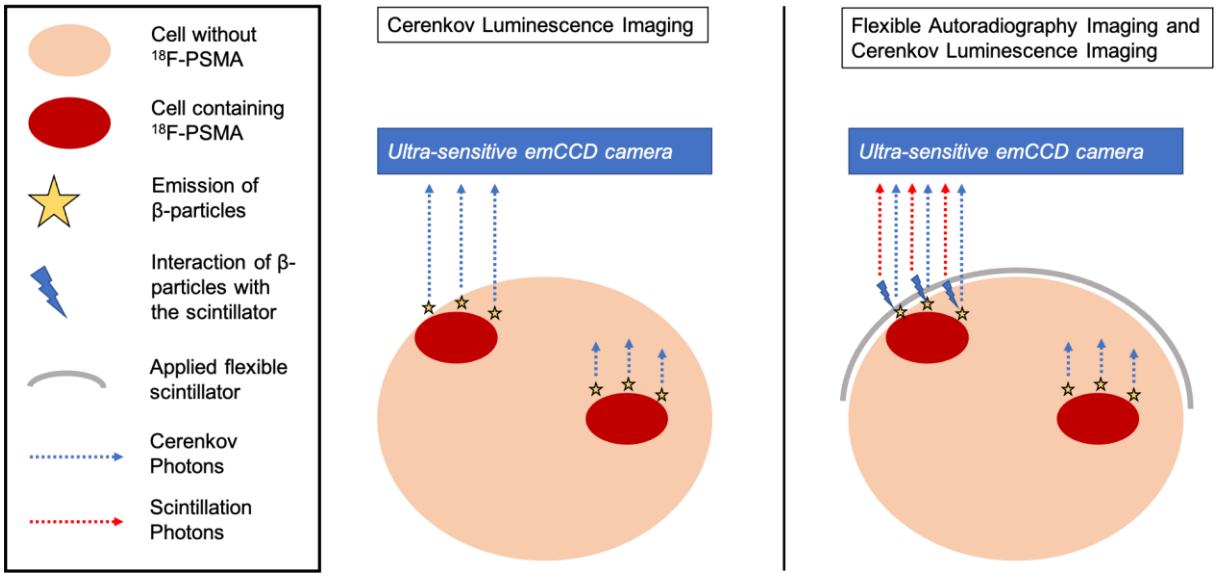

Schematic representation of Cerenkov Luminescence Imaging on the left and Flexible Autoradiography and Cerenkov Luminescence Imaging on the right using a flexible scintillating film. Tumor cells binding ^{18}F-PSMA emit β+-particles, which in turn emit Cerenkov optical photons or which are converted to scintillation photons by the flexible scintillator. As β+-particles travel a limited distance in tissue, ^{18}F-PSMA containing cells are detected only near the surface. The photons (Cerenkov photons and scintillation photons) are measured by an ultra-sensitive emCCD camera.

Supplemental Figure 2

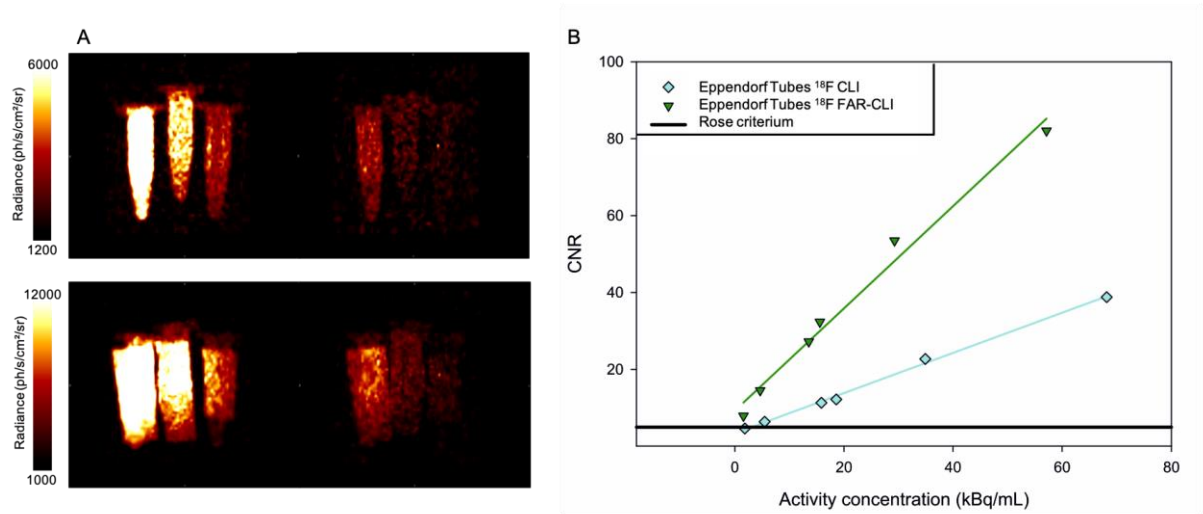

CLI (panel A top row) and FAR-CLI (panel A bottom row) radiance (photons/s/cm2/sr) of 18F solutions in Eppendorf tubes. Through dilution series (using distilled water), activity concentrations (AC) between 66.2 - 1.9 kBq/ml for CLI and 57.13 - 1.6 kBq/ml for FAR-CLI were examined. A illustrates the 3 highest ACs on the left, from outside to inside and the lowest 3 ACs on the right, from inside to outside; see panel B. Linearity and minimum detectable activity concentration are shown in panel B.

Supplemental Figure 3

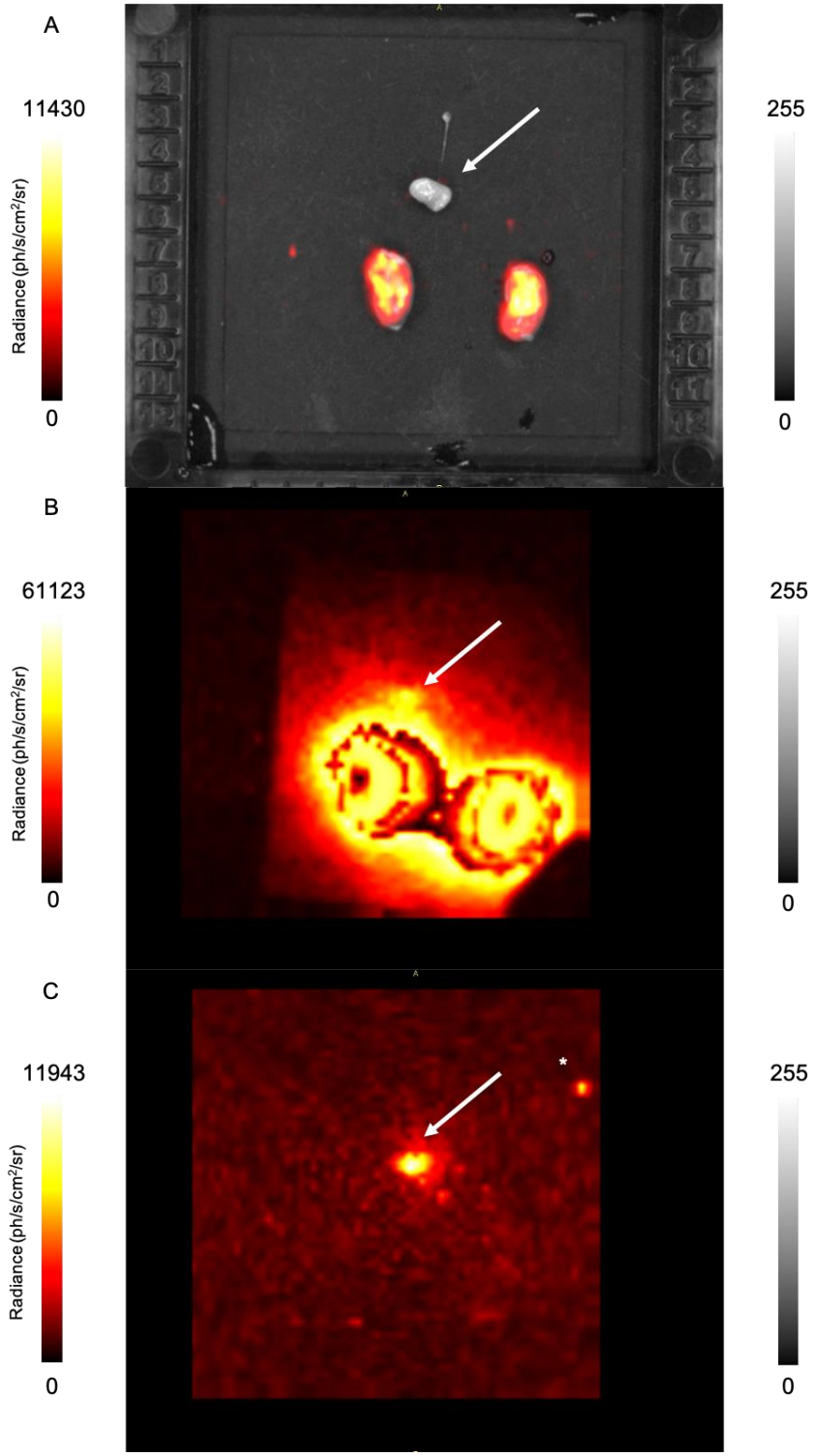

Gray-scale photographic images overlaid with CLI signals of the two mouse kidneys at the bottom and prostate cancer (PC) tissue at the top (A). In FAR-CLI (B) the PC signal cannot be clearly delineated (arrow) due to the strong radiation of the kidneys; thus, a separate image was taken only from PC. FAR-CLI showed a good signal of PC with a contrast-to-noise ratio of 20.16 and an activity of 7.85 kBq/ml; the asterisk marks an artificial signal (C).

Supplemental Figure 4

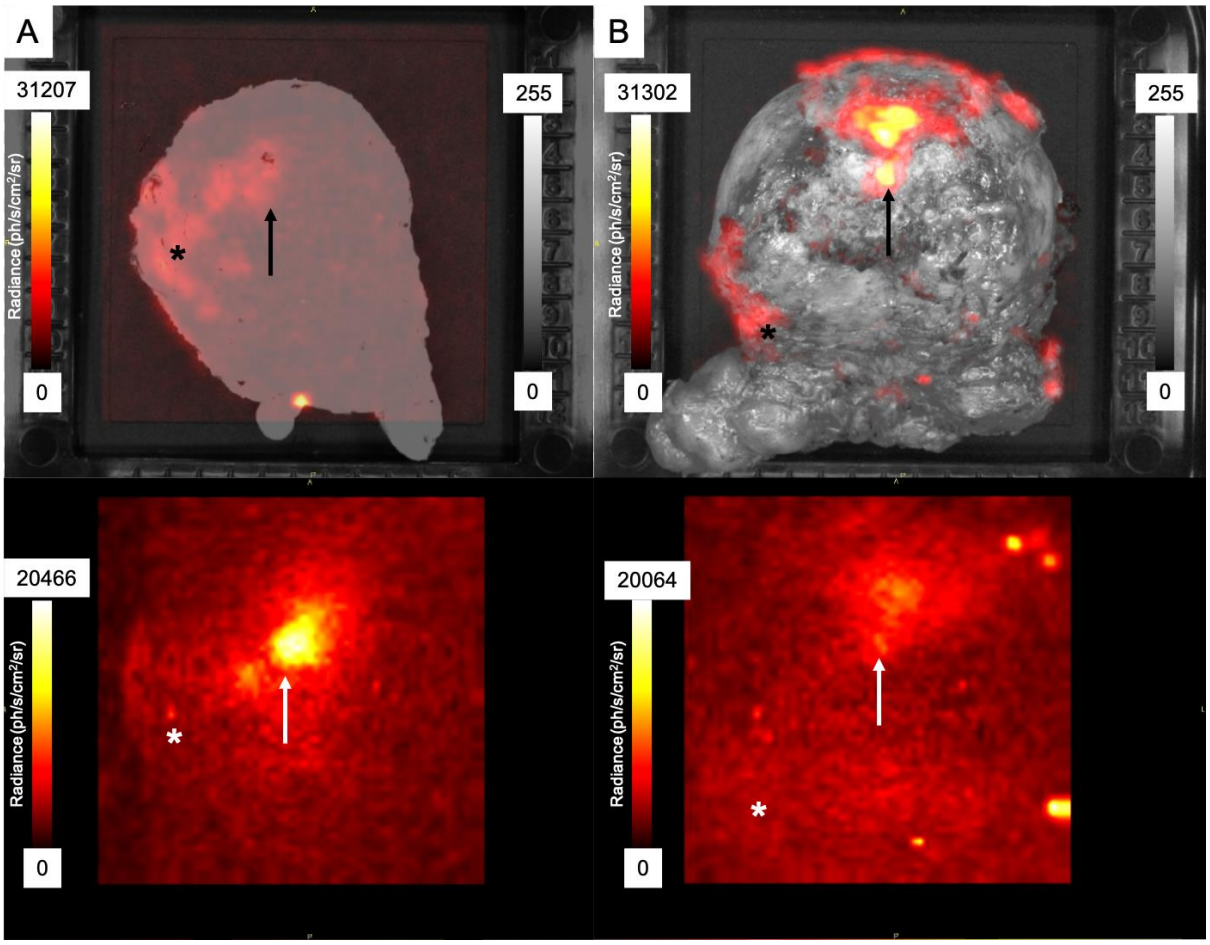

Gray-scale photographic images overlaid with Cerenkov signals (CLI, A+B top) and Flexible Autoradiography (FAR-CLI, A+B bottom) of two intact prostate specimens with histopathological proven positive resection margins (PRM). The area of the PRM is marked with a black asterisk * for CLI and a white asterisk * for FAR-CLI. Hotspots in FAR-CLI are indicated by white arrows, with the corresponding area in CLI indicated by black arrows. In images A, histopathology showed a PRM apically dorsal left, without corresponding photon signals. In images B, histopathology showed a PRM at the left seminal vesicle plateau, but a corresponding image signal could only be derived at the ventral prostate surface.

Supplemental Figure 5

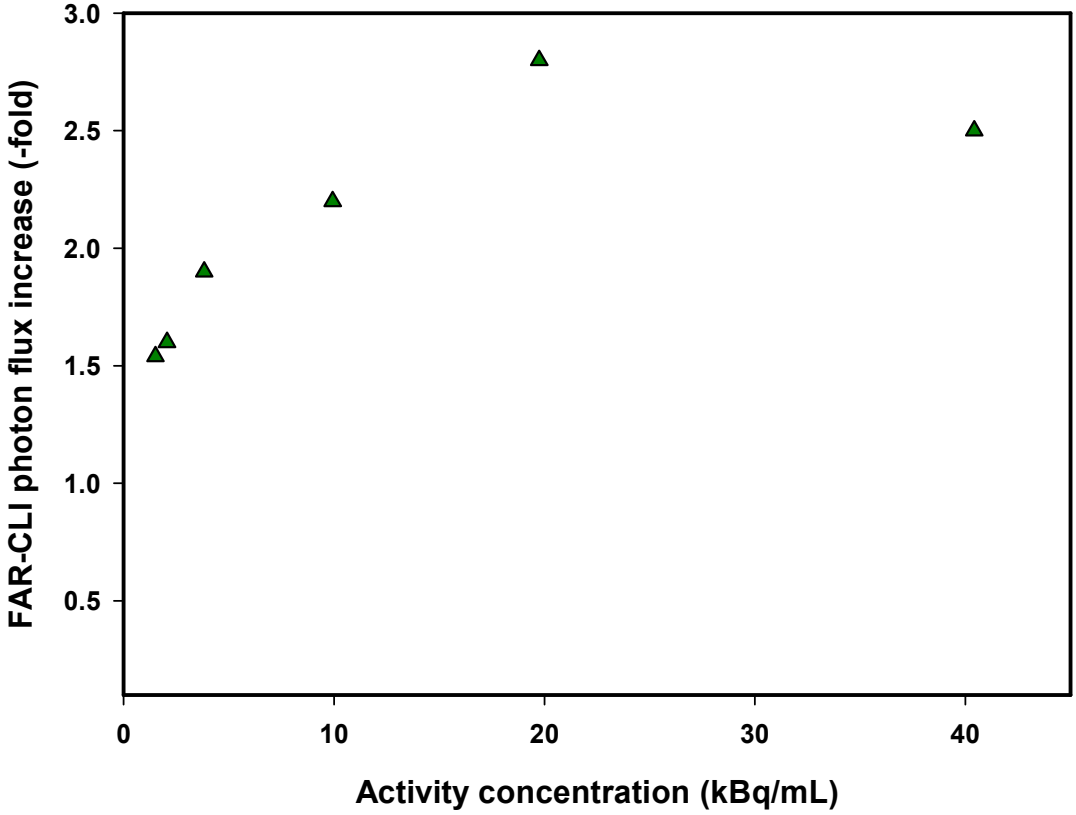

Radiance enhancement of FAR-CLI relatively to CLI in Eppendorf tubes filled with ^{18}F. Here the background corrected radiance levels were normalised to the activity concentration, decay corrected to the time-point of measurement.